Drop vaporization frequency response: an approximate analytical solution for mixed injection regimes

Kwassi Anani, Roger Prud'homme, Mahouton Norbert Hounkonnou

Drop vaporization frequency response: an approximate analytical solution for mixed injection regimes

Kwassi Anani[1,*], Roger Prud'homme[2] and Mahouton Norbert Hounkonnou[3]

[1]*Doctor, Laboratory of Mathematical Modelling and Applications, Department of Mathematics, Faculty of Sciences, University of Lomé, 02 BP 1515 Lomé, Togo; Tel.: (+228) 90 15 91 36; Fax: (+228) 22 21 85 95 ORCID iD: https://orcid.org/0000-0001-6679-4569 - E-mail: kanani@univ-lome.tg*

[2]*Emeritus Research Director, Jean Le Rond d'Alembert Institute, UMR 7190 - Sorbonne University / Centre National de la Recherche Scientifique - Box 162 - 4 place Jussieu - 75252 Paris Cedex 05- E-mail: roger.prud_homme@courriel.upmc.fr*

[3]*Professor, University of Abomey-Calavi, International Chair in Mathematical Physics and Applications (ICMPA-UNESCO Chair) 072 B.P. 050 Cotonou, Republic of Benin- E-mail: norbert.hounkonnou@cipma.uac.bj*

DOI : 10.21494/ISTE.OP.2021.0748

Abstract

This work is devoted to a theoretical analysis of evaporating mass frequency response to pressure oscillations of a spray of repetitively injected drops into a combustion chamber. A single stationary spherical droplet continuously fed with the same liquid fuel, so that its volume remains constant in spite of the evaporation, the so-called 'mean droplet' in the Heidmann analogy, represents this vaporizing spray of droplets. The feeding is realized with a liquid-liquid heat transfer coefficient by using a source point placed at the mean droplet centre, in such a way that only radial thermal convection and conduction effects are allowed inside the droplet during the process. This feeding procedure is now viewed as a proper boundary condition that is a mixed or a generalized feeding regime controlling the whole process of liquid fuel injection into the combustion chamber. Drawing upon a linear analysis based on the Rayleigh criterion, the evaporating mass response factor is evaluated. Effects due to the variation of the heat transfer coefficient and of the process characteristic times are analysed. Especially, an abrupt increase in the response function is related to the influence of the value of a particular fuel thermodynamic coefficient.

Keywords: combustion instability; heat exchange ratio; truncated expansion; double confluent Heun equation; transfer function

[*]Corresponding author. Email: kanani@univ-lome.tg

1 Introduction

Combustion instabilities still nowadays a challenging area in combustion research though their modelling and control have been investigated in many published works by various research teams during the past decades. Combustion instabilities result from the coupling between acoustic waves and combustion. In confined devices, the coupling between acoustic field and heat or mass release at certain frequency levels may lead to engine failure or other catastrophic consequences [1, 2]. On the contrary, new blends of fuels can be engineered to undergo preferential instabilities leading to homogeneous combustion with higher efficiency [3]. Combustion instabilities can occur in both premixed and diffusion flames. The present study is mostly concerned with subcritical diffusion flame models. In these latter, many causes were identified as being responsible for exciting or damping the mass release frequency response [4, 5]: period of ambient pressure oscillations which is closely related to the combustion chamber geometry, liquid fuel injection and atomization mechanisms with diverse boundary conditions, vaporization characteristic times that are obviously dependent on thermal convection and conduction processes, etc.

Compared with the other processes associated with combustion chamber, vaporization has been pointed as the slowest [6], and hence may be the rate-controlling process. The evaporating mass frequency response of droplets to ambient pressure oscillations are generally computed by using classical droplet evaporation theories [3], on the basis of the Rayleigh criterion [7], by assuming simplifying assumptions. Most of the theoretical studies in the area are based on single vaporizing droplet models as for example [6, 8, 9]. Then, by means of numerical simulations, the dynamic response of the vaporization frequency response of spray droplets to ambient pressure oscillations can be taken as a statistical consequence of the vaporization characteristics of each individual droplet in the array. Among previous numerical works on vaporization frequency response of sprays, Tong and Sirignano [10] examined the effects of oscillating gas pressure and velocity on vaporization rates of continuously injected droplets during combustion instability. They concluded that self-sustained acoustical oscillations can occur in the combustor when vaporization is a controlling phenomenon. More recently, de la Cruz Garc’ıa et al. [11] investigated on the self-excited oscillations in a kerosene spray flame and concluded that the combustor stability strongly depends on the fuel distribution, degree of evaporation, and mixing before the main reaction zone. Progress has also been made in analytical modelling of vaporization frequency response of spray droplets. Haddad and Majdalani [12] provided a closed-form analytical solution for the transverse vorticoacoustic wave in a circular cylinder with headwall injection. Likewise, researchers have recently reported improved analytical models for spray combustion instability in diverse configurations as for example Greenberg and Katoshevski (see [13] and references therein). In all the above-mentioned studies, the actual changing volume due to the vaporization of the injected droplets has been taken into account.

One of the analytical approaches for evaluating the vaporization frequency response of spray droplets can stem from Heidmann analogy of a spherical vaporizing droplet of constant volume [14]. This configuration consists of representing the spray of repetitively injected drops in the combustion chamber by a motionless mean droplet. The single vaporizing droplet is continuously supplied at a stationary flow rate with the same liquid fuel. This classical model can permit to include most of the above-mentioned mechanisms that intervene in combustion instability phenomena, in a single theoretical analysis. Heidmann and Wieber first based their model on the hypothesis that, the mean spherical droplet summarizes the oscillatory rate of vaporization of an array of repetitively injected droplets in the combustion chamber [14]. However, an infinite thermal diffusivity of the liquid phase is

assumed, and the mean droplet has a uniform temperature whatever the feeding process adopted. This classical model was refined by Prud'homme et al. [15]. A finite thermal diffusivity of the liquid is taken into account but, the feeding process at the mean droplet centre is assumed adiabatic, and the radial thermal convection term that appears in the energy equation of the liquid phase is neglected (pure conduction model). In [16], Anani and Prud'homme extended the study of this pure conduction model by taking into account the isothermal feeding process at the mean droplet centre. Recently, an approximate analytical model has been performed by Anani et al. [17] where was relaxed the simplifying assumption of a negligible radial thermal convection effect inside the liquid phase. Nevertheless, only the two extreme cases of centre injection that are the adiabatic and the isothermal feeding regimes were considered. Apart from this latter work, no analytical solution has been found and any asymptotical study has been performed for intermediate injection cases where the feeding regime at the mean droplet centre is a combination of the two extreme thermal forcing types.

The present paper aims at contributing to the linear analysis of subcritical combustion instabilities by analytical approaches based on the mean spherical droplet configuration as in [17]. In the following section, a brief description is given of the unperturbed state corresponding to the vaporization of the continuously fed spherical droplet in a stable environment. In section 3, the linear analysis for harmonic perturbations in pressure is performed and a double confluent Heun equation (see [18]) is derived from the energy equation of the liquid phase. Then, an approximate analytical expression of the temperature field inside the mean droplet is obtained for the generalized or mixed injection regime and the mass response factor is defined. Results are discussed in section 4. Throughout the discussion, comparisons are made with certain results of models in the literature that account for the actual changing volume due to vaporization of individual injected droplets in the spray. Finally, key results are recalled in the conclusions.

2 Stabilized state description

2.1 General assumptions

Individual spherical fuel droplets are repetitively injected into a subcritical combustion chamber. The distance between the droplets is supposed large enough, so that no interaction occurs between the droplets or between the droplets and the wall. Assuming velocity-stabilized hypotheses as in [14], the vaporizing spray of droplets is represented by an idealized physical configuration of a mean spherical droplet at rest in the combustion chamber. The mean droplet, placed at a specific location in the combustion chamber (pressure anti-node and velocity node), is supposed to summarize the frequency response of individual drops in the spray. The vaporizing mean droplet has a constant average radius $\overline{r}_S$, since its instantaneous evaporating mass m is continuously restored with the average mass flow rate $\overline{m}$ of the same fluid, by using a point source placed at the droplet centre. The choice of the Arithmetic Mean Diameter configuration is motivated by the analytical approach of the problem, since it leads for the mean droplet to conservation equations with fixed boundary conditions. From now on, all barred quantities indicate mean values corresponding to the stabilized state, whereas all primed quantities will denote relative perturbation quantities i.e. $x' = (x - \overline{x}) / \overline{x}$.

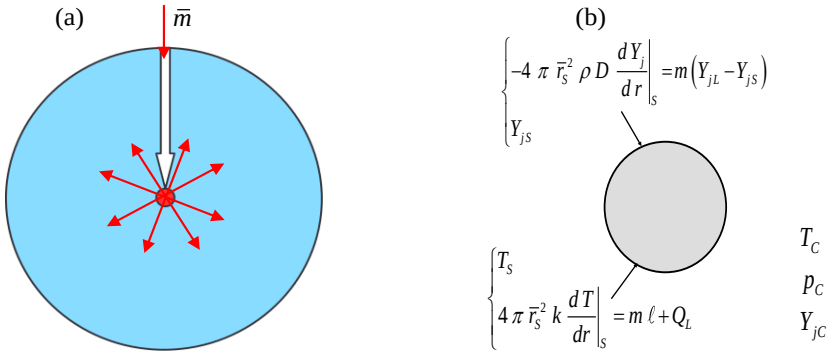

Figure 1. (a) The mean vaporizing droplet, continuously fed by a point source placed at its centre. (b) Boundary conditions for the supplied droplet.

The local feeding rate $\bar{m}$ is distributed throughout the droplet (see Figure 1(a)) in such a way that, except for the radial thermal convection effect from the droplet centre to its evaporation surface, any other convective transport or liquid recirculation phenomenon within the droplet is negligible. The spherical shape of the mean droplet is maintained at every moment during the process, and the thermal dilatation of the liquid is negligible so that the density ρ_L, the specific heat c_L and the thermal conductivity k_L of the droplet will be treated as constant. A generalized or mixed boundary condition is considered at the mean droplet centre, that is, the liquid fuel is injected with a positive heat transfer coefficient h. The two extreme cases of this injection process are the adiabatic feeding regime ($h = 0$) where zero temperature gradient is assumed at the droplet centre, and the isothermal feeding regime ($h = \infty$) where the droplet centre is kept at the constant temperature $\bar{T}_S$. The latter is the mean value of the spatially uniform but time-varying temperature T_S of saturated vapour at the stabilized droplet surface.

In the immediate vicinity of the droplet surface, the gas phase is made up of stoichiometric reaction products evolving in a quasi-steady state. Equilibrium conditions at the droplet/gas interface are assumed for the stabilized state and there is no gas diffusion into the droplet. Far from the mean droplet, the ambient environment of the chamber is at constant subcritical temperature T_C and pressure p_C. The boundary conditions at the mean droplet surface are shown in Figure 1(b). Subscripts L and l refer to the liquid phase, whereas subscripts S and C respectively indicate the droplet surface and the ambient conditions of the combustion chamber far from the droplet. The heat flux transferred to the liquid is designated by Q_L and the binary diffusion coefficient of fuel vapour in air is denoted by D. The density and the thermal conductivity of the gas mixture around the droplet surface are respectively designated by ρ and k. The gaseous mixture near the surface is composed of fuel species $j = F$ and of combustion products diluted species $j = A$ proceeding from the flame front at infinity. By denoting the mass fraction of species j as Y_j, a mono-component droplet with only fuel species will be considered for reason of simplicity, that is $Y_{FL} = 1$ and $Y_{AL} = 0$.

Theoretical studies of the evaporating mass response of spray droplets to acoustic and/or velocity perturbations in combustors are mostly based on numerical simulations. But, even while assuming certain simplifying assumptions, analytical models that include more complex aspects of the problem are needed for providing deep insights in the vaporization

frequency response. Those analytical approaches may then serve to improve the development of numerical codes, as for instance Computational Fluid Dynamic (CFD) codes. Nevertheless, both numerical and analytical models need to be confronted with appropriate experimental measurements and more detailed validation databases for validating the predictions. Specifications of an experimental design may include several regulations and measurement devices [19]. As the present theoretical study is based on the mean droplet configuration, experimental facility and methods similar to those described in [20] can provide tracks for some experiments. However, the problem is here considered only under its analytical aspect. As mentioned in the introduction, the mean droplet model can permit including most of the mechanisms that intervene in spray combustion instability, in a single theoretical analysis. Therefore, results obtained through approximate analytical solutions are still extendable to more complex configuration details. The results may then serve as references for full experimental and numerical simulations of spray combustion instability which will not need to rely on the simplifying assumptions necessarily adopted here.

2.2 Characteristic times

The characteristic times controlling heat transfer processes inside the stabilized mean spherical droplet are the residence time and the transfer time by thermal diffusion. The residence time of the continuously fed droplet can be equated with the mean lifetime of an individual vaporizing droplet in the spray. This time replaces the notion of a free droplet lifetime in the present situation of constant volume and is identified to the ratio $\bar{\tau}_v = \overline{M} / \bar{m}$, where $\overline{M}$ represents the mean value of the actual mass M of the supplied droplet and $\bar{m}$ is the stationary feeding rate. The transfer time by thermal diffusion process is defined as $\bar{\tau}_T = \bar{r}_S^2 / \kappa_L$, where $\kappa_L = k_L /(\rho_L c_L)$ is the thermal diffusivity of the liquid and $\bar{r}_S$ the constant average radius. It is then convenient to use the timescale ratio $\theta = 9\bar{\tau}_v / \bar{\tau}_T$, which will be called from now on, the thermal exchange ratio or more briefly the exchange ratio, as it is of the same order of magnitude as $1/Pe_L$, Pe_L being the Péclet number of the liquid phase. The coefficient 9 permits to obtain later a simple expression of the transfer function and will be kept for comparison purposes with results obtained in previous studies [16, 17]. During the vaporization, intrinsic or external pressure-related oscillations can cause departure from stabilized-state conditions. In the case of small harmonic perturbations in pressure, a linear analysis can be performed. The wave period of these ambient pressure oscillations is a major characteristic time of the process. The frequency of the harmonic oscillations in ambient pressure will be denoted by ω. In the first study of the mean droplet [14], the response functions were evaluated over fairly wide range of flow conditions. The data was found to be correlated with a dimensionless parameter, which is the droplet lifetime or half lifetime normalized by the wave period. In the same order, a reduced frequency u depending on the residence time $\bar{\tau}_v$ and defined as $u = 3\omega\bar{\tau}_v$ will be considered. Here again, the coefficient 3 is kept for simplifying later expression of the transfer function and for comparison purposes with results obtained in previous studies [16, 17].

2.3 Unperturbed state equations

The mass balance of the mean droplet can be written:

$$\frac{\mathrm{d}M}{\mathrm{d}t} = \bar{m} - m$$

(1)

with $\bar{m}$ and m denoting respectively the stationary flow of injection and the instantaneous flow of evaporation. In a stabilized state, one has: $m \equiv \bar{m}$, $\mathrm{d}M/\mathrm{d}t = 0$ and $M = \overline{M}$. The amount of heat Q_L penetrating into the droplet is expressed as:

$$4\pi \bar{r}_S^2 \, k_L \left. \frac{\partial T_l}{\partial r} \right|_{\bar{r}_S, t} = Q_L = Q - m\ell \qquad (2)$$

where $T_l \equiv T_l(r,t)$ is the temperature value at radial coordinate r and at time t inside the mean droplet, Q is the external gas heat flux and ℓ the latent heat of vaporization per unit mass of the liquid. Equation (2) assures the coupling of the gas and the liquid phase solutions at the mean droplet surface. As the energy conservation equation includes both radial thermal convection and conduction data, the internal temperature T_l satisfies the following equation:

$$\rho_L \, c_L \frac{\partial \, T_l}{\partial t} + \rho_L \, c_L v_r \frac{\partial T_l}{\partial r} - \frac{k_L}{r} \frac{\partial^2 \left(r \, T_l \right)}{\partial \, r^2} = 0 \qquad (3)$$

where v_r is the central injection velocity expressed as $v_r = \bar{m} / 4\pi\rho_L r^2$; $0 < r < \bar{r}_S$. Equation (3) is subject to a mixed boundary condition at the droplet centre and to the Dirichlet boundary condition at the surface:

$$\begin{cases} \left. \dfrac{\partial T_l}{\partial r} \right|_{r=0,t} = \dfrac{h}{\bar{r}_S} \left(T_l(0,t) - \bar{T}_S \right) \\ T_l(\bar{r}_S, t) = T_S(t) \end{cases} \qquad (4)$$

The parameter $h > 0$ in Equation (4) indicates the heat transfer coefficient. We recall that, $h = 0$ and the mixed boundary condition is reduced to $\partial T_l(0,t)/\partial r = 0$ for the adiabatic injection centre, whereas $h = \infty$ and the same condition becomes $T_l(0,t) = \bar{T}_S$ for the isothermal injection centre. The mixed boundary condition at the droplet centre can be viewed as an idealized modelling of a specifically preheated spray injection process. In real liquid fuel injection processes, internal flow evaluations depend on inlet boundary conditions (see [21] or references therein). Some studies have shown that the reduction in kinematic viscosity resulting from fuel preheating improves the combustion and emissions performance of the engine [22, 23]. Now, in subcritical combustion systems, the two extreme cases bounding the possible range of a real inlet liquid temperature fluxes are precisely the adiabatic and the isothermal feeding regimes. The adiabatic feeding regime at the mean droplet centre can be related to an unheated spray feeding process where the mean temperature $\overline{T_A}$ of the injected fuel is connected to standard conditions for temperature and pressure. On the contrary, the isothermal feeding regime can be taken into account by assuming the injected fuel at the mean temperature $\overline{T_S}$ of the vaporizing droplet surface. This injected fuel temperature $\overline{T_S}$ for the isothermal regime can be related to the liquid wet bulb temperature T_{WB} or to its boiling temperature T_B when T_{WB} estimate is unavailable [24]. Therefore, in an actual mixed injection process, an inlet fuel temperature may be stated between the extreme values that are $\overline{T_A}$ and $\overline{T_S}$. During the combustion process, the

corresponding rate of heat brought by the injected fuel to the vaporizing array of droplets can be investigated by means of a heat transfer coefficient. The present model of a representative spherical droplet fed by a mass and heat point source placed at its centre includes among other advantages, the possibility to formulate the boundary conditions (Equation (4)) with a heat transfer coefficient $h > 0$. Now, contrary to the classical adiabatic condition, the mixed boundary condition doesn't assure the regularity of the heat flux at the droplet centre and the spherical shape of the mean droplet is no more guaranteed in this feeding regime. Nevertheless, we assume for both feeding regimes that the mean droplet remains spherical with a fixed size during the feeding process. The radial liquid velocity diverges at the mean droplet centre, even in the adiabatic feeding regime where this infinite divergence is counterbalanced by a zero heat flux at the centre. However, in both adiabatic and mixed feeding regimes, the evaluation of the mass response factor only depends on the regularity of the internal temperature field at the mean droplet surface. Thus, using simplifying assumptions, the present study aims at providing such regular approximate analytical solutions, in order to investigate the effect of a heat transfer coefficient, related to fuel injection processes, on the vaporization frequency response.

Assuming quasi-steady hypotheses, the droplet surface is at local evaporation equilibrium and the instantaneous mass vaporization rate can be calculated as:

$$m = 2\pi \rho D r_S \, Sh^* \ln(1+B_M) = 4\pi \frac{k}{c_p} r_S \, Nu^* \ln(1+B_T) \tag{5}$$

where $B_M = (Y_{FS} - Y_{FC})/(1-Y_{FS})$ and $B_T = c_p(T_C - T_S)/(\ell + Q_L/m)$ are the well-known Spalding mass and heat transfer numbers, and c_p the specific heat capacity of fuel vapour at constant pressure. As mentioned above, parameters ρ, k, and D are the density, the thermal conductivity and the binary diffusion coefficient of the mixture of vapour and ambient gas. The Sherwood and Nusselt numbers Sh^* and Nu^* were provided by Abramzon and Sirignano in their extended film model [25]. At the droplet surface, the saturated vapour pressure can be expressed as $p_{sat}(T_S) = \exp\left(a - b/(T_S - c)\right)$ with a, b and c being some coefficients related to the fuel thermophysical properties. The pressure p_{sat} and the mole fraction X_{FS} of fuel species are connected by the relation $p\,X_{FS} = p_{sat}(T_S)$, where $p = p_C$ denotes the ambient pressure. If the molecular weight of species j (= A or F) is denoted by M_j, then the mass fraction Y_{FS} of the vapour at the droplet surface can be written as a function of the mole fraction X_{FS} as:

$$Y_{FS} = \frac{\mathrm{M}_F}{\mathrm{M}_F X_{FS} + \mathrm{M}_A X_{AS}} X_{FS} \tag{6}$$

Since concentrations and temperature values are varying in the gas phase, the averaged properties can be evaluated at some reference concentration $\overline{Y}_j = Y_{jS} + A_r\left(Y_{jC} - Y_{jS}\right)$ and temperature $\overline{T} = T_S + A_r\left(T_C - T_S\right)$ with $A_r = 1/3$. Both Sh^* and Nu^* are assumed equal to two and the Lewis number $Le = k/\rho D c_p$ is equal to one.

3 Linear analysis for small perturbations

3.1 Linear analysis of the liquid-phase equations

Splitting up the flow variables into steady and unsteady parts can be realized by writing $\Delta f = f - \overline{f}$, where f is a flow parameter, $\overline{f}$ is its mean value, Δf is the absolute perturbation, and $f' = \Delta f / \overline{f}$ is the corresponding relative perturbation. The heat flow at the surface, Equation (2), is then given by:

$$4\pi\, \overline{r}_S^{\,2}\, k_L \overline{T}_S \left.\frac{\partial T_l^{'}}{\partial r}\right|_{\overline{r}_S,t} = Q_L - \overline{Q}_L = Q_L = \Delta Q_L \tag{7}$$

as $\overline{Q}_L = 0$. The energy conservation equation (Equation (3)) can be rewritten for the perturbed temperature $T_l^{'}(r,t) = [T_l(r,t) - \overline{T}_l(r,t)] / \overline{T}_l(r,t)$ as:

$$\frac{\partial (r\, T_l^{'})}{\partial t} + \kappa_L \left(\frac{3\overline{r}_S}{\theta r} \frac{\partial T_l^{'}}{\partial r} - \frac{\partial^2 (r\, T_l^{'})}{\partial\, r^2} \right) = 0 \tag{8}$$

where $\theta = 9\overline{\tau}_v / \overline{\tau}_T$ is the thermal exchange ratio defined in section 2. The perturbed boundary conditions in the mixed feeding regime are deduced from Equation (4) as follows:

$$\begin{cases} \left.\dfrac{\partial T_l^{'}}{\partial r}\right|_{r=0,t} = \dfrac{h}{\overline{r}_S} T_l^{'}(0,t) \\ T_l^{'}(\overline{r}_S,t) = T_S^{'}(t) \end{cases} \tag{9}$$

Introducing now small harmonic perturbations of frequency ω in the form of $f' = \hat{f}(r)\exp(\mathrm{i}\omega t)$, the ambient pressure, temperature and heat transferred into the droplet are respectively expressed as $p' = \hat{p}_C \exp(\mathrm{i}\omega t)$, $T_l^{'} = \hat{T}_l(r)\exp(\mathrm{i}\omega t)$ and $\Delta Q_L = \Delta \hat{Q}_L(r)\exp(\mathrm{i}\omega t)$. Equation (8) is then transformed into:

$$\mathrm{i} r^2 \omega \hat{T}_l + \frac{3\kappa_L \overline{r}_S}{\theta} \frac{\mathrm{d}\hat{T}_l}{\mathrm{d}r} - \kappa_L r \frac{\mathrm{d}^2 (r\hat{T}_l)}{\mathrm{d}r^2} = 0 \tag{10}$$

or equivalently into:

$$\mathrm{i}\omega \overline{\tau}_T \xi \hat{T}_l + \frac{1}{3\theta\xi} \frac{\mathrm{d}\hat{T}_l}{\mathrm{d}\xi} - \frac{\mathrm{d}^2 (\xi \hat{T}_l)}{\mathrm{d}\xi^2} = 0 \tag{11}$$

where $\hat{T}_l$ is taken as a function of the reduced radius variable $\xi = r / \overline{r}_S$, $(0 < \xi < 1)$. The boundary conditions in the generalized feeding regime, Equation (9), can then be written in connection with ξ as:

$$\begin{cases} \left.\dfrac{\mathrm{d}\hat{T}_l}{\mathrm{d}\xi}\right|_{\xi=0} = h\hat{T}_0 \\ \hat{T}_l(1) = \hat{T}_S \end{cases} \tag{12}$$

where $\hat{T}_0$ depends on the initial temperature of the injected liquid fuel.

We now consider the complex number $\bar{s}_0 = (1-\mathrm{i})(\omega/2\kappa_L)^{1/2}$, conjugate of $s_0 = (1+\mathrm{i})(\omega/2\kappa_L)^{1/2}$, s_0 and $-s_0$ being the roots of the characteristic equation $\mathrm{i}\omega - \kappa_L s^2 = 0$ obtained from Equation (11), when neglecting the convective term $(1/3\theta\xi)\mathrm{d}\hat{T}_l/\mathrm{d}\xi$. For a given value of the positive heat transfer coefficient h, a solution of Equation (11) subject to Equation (12) can be sought in the form of $\xi\hat{T}_l(\xi) = J(\xi)\{1-\cos[\bar{s}_0\bar{r}_S\xi\exp(\mathrm{i}\arctan h)]\}$, with $\exp(\mathrm{i}\arctan h) = (\mathrm{i}h+1)/(h^2+1)^{1/2}$, and J referring to a function to be determined. From the second-order truncated expansions of sine and cosine functions that are $\sin(S_0\xi)\approx S_0\xi$ and $\cos(S_0\xi)\approx 1-(S_0\xi)^2/2$ by writing $S_0 = \bar{s}_0\bar{r}_S\exp(\mathrm{i}\arctan h)$, it is deduced that the function ξJ approximately verifies the following double confluent Heun equation:

$$\xi^2\frac{\mathrm{d}^2(\xi J)}{\mathrm{d}\xi^2}+\left(2\xi-\frac{3}{\theta}\right)\frac{\mathrm{d}(\xi J)}{\mathrm{d}\xi}-2\bar{s}_0^2\bar{r}_S^2\frac{h(\mathrm{i}-h)}{h^2+1}\xi^2(\xi J)=0 \tag{13}$$

By using the Maple notation, a solution of Equation (13) can be expressed as $J(\xi) = C_0\exp(-3(\theta\xi)^{-1})\,\mathrm{HeunD}(x_1,x_2,x_3,x_4,x)/\xi^{\frac{5}{2}}$, where C_0 is an arbitrary constant and $\mathrm{HeunD}(x_1,x_2,x_3,x_4,x)$ is the double confluent Heun function with its corresponding four parameters: $x_1 = 0$, $x_2 = -[\theta^2(h^2+1)-9-9h^2-24uh(\mathrm{i}h+1)\theta]/4\theta^2(h^2+1)$, $x_3 = -[9+(9-24\mathrm{i}u\theta)h^2-24hu\theta]/2\theta^2(h^2+1)$ and $x_4 = -[-\theta^2(h^2+1)-9-9h^2-24uh(\mathrm{i}h+1)\theta]/4\theta^2(h^2+1)$. The variable x is expressed in function of ξ as $x = (\xi^2-1)/(\xi^2+1)$. We recall that the quantity $u = 3\omega\bar{\tau}_v$ is the ambient pressure frequency defined in the precedent section. Thus, for the mixed feeding regime, the boundary condition $\hat{T}_l(1) = \hat{T}_S$ at the mean droplet surface leads to the following approximate analytical solution:

$$\hat{T}_l(\xi) = \exp\left(\frac{3}{2\theta}\left(1-\frac{1}{\xi}\right)\right)\frac{\hat{T}_S\{1-\cos[\exp(\mathrm{i}\arctan h)\,\bar{s}_0\bar{r}_S\xi]\}\,\mathrm{HeunD}\left(x_1,x_2,x_3,x_4,\dfrac{\xi^2-1}{\xi^2+1}\right)}{\{1-\cos[\exp(\mathrm{i}\arctan h)\,\bar{s}_0\bar{r}_S]\}\xi^{\frac{5}{2}}} \tag{14}$$

This approximate analytical solution presents an essential discontinuity at $\xi = 0$, since the temperature gradient is not null at the droplet centre when $h > 0$. Now, the calculation of the mass response factor only includes regularity conditions at the droplet surface $\xi = 1$ and these conditions are well verified by the solution expressed in Equation (14). Thus, the flow condition at the droplet surface (Equation (7)) can be written as $4\pi\bar{r}_S k_L\bar{T}_S\left.\dfrac{\mathrm{d}\hat{T}_l}{\mathrm{d}\xi}\right|_{\xi=1} = \Delta\hat{Q}_L$ and then be applied to the solution in Equation (14). That leads to:

$$\Delta\hat{Q}_L = -4\pi\bar{r}_S\,k_L\bar{T}_S\hat{T}_S E\left(u,\theta,h\right) \tag{15}$$

where E is expressed in function of u , θ and h as:

$$E\left(u,\theta,h\right) = \bar{s}_0\bar{r}_S\exp(\mathrm{i}\arctan h)\frac{\sin[\exp(\mathrm{i}\arctan h)\bar{s}_0\bar{r}_S]}{\cos[\exp(\mathrm{i}\arctan h)\bar{s}_0\bar{r}_S]-1}-\frac{3}{2\theta}+\frac{5}{2} \tag{16}$$

with $\bar{s}_0\bar{r}_S = (1-\mathrm{i})(3u/2\theta)^{1/2}$, $u = 3\omega\bar{\tau}_v$ and $\theta = 9\bar{\tau}_v/\bar{\tau}_T$.

3.2 Gas-phase linearized equations

The linearized equations for the liquid/gas interface initially presented in [15] and used in [16, 17], are here briefly recalled. Introducing the harmonic perturbations, the ambient pressure is given by $p' = \hat{p}_C \exp(\mathrm{i}\omega t)$ and the perturbed mass flow rate will take the form of $m' = \hat{m} \exp(\mathrm{i}\omega t)$. Consequently, the equations of the gas phase (see subsection 2.3) imply:

$$\hat{m} = \alpha \frac{\mathrm{i}u}{1 + \mathrm{i}u} (\bar{b}\, \hat{T}_S - \hat{p}_C) \tag{17}$$

and

$$\Delta \hat{Q}_L = \bar{m}\, \bar{\ell}\ (\bar{a} \hat{p}_C - \mu \hat{T}_S) \tag{18}$$

where $u = 3\omega\bar{\tau}_v$ and $\Delta Q_L = \Delta\hat{Q}_L \exp(\mathrm{i}\omega t)$. The coefficients involved in these equations are:

$$\bar{a} = \frac{\bar{T}_C}{\bar{T}_C - \bar{T}_S} \frac{\gamma - 1}{\gamma} + \varphi, \quad \bar{b} = \frac{\bar{T}_S}{(\bar{T}_S - c)^2}\, b, \qquad \mu = \frac{\bar{T}_S}{\bar{T}_C - \bar{T}_S} - \frac{2c}{\bar{T}_S - c} + \bar{b}\varphi \qquad \text{and}$$

$$\alpha = \frac{\bar{B}_M}{(1 + \bar{B}_M)\ \ln(1 + \bar{B}_M)}\ \varphi \quad \text{where} \quad \varphi = \frac{\bar{Y}_{AC}\bar{Y}_{FS}}{\bar{Y}_{AS}(\bar{Y}_{FS} - \bar{Y}_{FC})}\ \frac{\mathrm{M}_F}{\mathrm{M}_F \bar{X}_{FS} + \mathrm{M}_A \bar{X}_{AS}}$$

The parameter γ stands for the constant isentropic coefficient and the latent heat of vaporization ℓ per unit mass of the liquid is given by $\ell = b R T_S^2 / \mathrm{M}_F (T_S - c)^2$, where R denotes the universal gas constant.

3.3 Mass response factor

It is assumed that the mean spherical droplet is at rest in the combustion chamber. The acceleration or velocity frequency response relatively to the ambient environment is negligible, and only the evaporating mass response due to the ambient acoustic forcing is considered. The mass response factor is studied by using a linear analysis for harmonic perturbations in pressure. According to the Rayleigh criterion, when the harmonic oscillations in pressure $p' = \left(p - \bar{p}\right)/\bar{p}$ induces a perturbation in the evaporating mass flow rate $q' = \left(q - \bar{q}\right)/\bar{q}$, the mass response factor N can be expressed as the ratio of the magnitude of the mass perturbation to the magnitude of the pressure perturbation:

$$N = \frac{\iint_{V,t} q'(V,t)\, p'(V,t) dt\, dV}{\iint_{V,t} (p'(V,t))^2\, dt\, d\mathrm{V}} \tag{19}$$

The double integral is taken over the wave period of time t in the finite volume V. Considering sinusoidal oscillations which are uniform over a finite volume, the response factor is defined as $N = (|\hat{q}|/|\hat{p}|)\cos\phi$, where $|\hat{q}|$ and $|\hat{p}|$ are the modules of mass release q' and pressure p', and ϕ is the phase difference between q' and p'. Therefore, a reduced mass response factor can be defined as the real part of the transfer function $Z = \hat{m}/(\alpha \hat{p}_C)$. By using Equations (15)-(18) the expression of Z is deduced in function of u, θ and h as:

$$Z(u,\theta,h)=\frac{\mathrm{i}u}{1+\mathrm{i}u}\,\frac{A+\theta E(u,\theta,h)}{B-\theta E(u,\theta,h)} \tag{20}$$

where $A=3(\bar{a}\bar{b}-\mu)/\lambda$ and $B=3\mu/\lambda$ are some coefficients depending on $\lambda=c_L\bar{T}_S/\bar{\ell}$ and are related to the fuel physical properties. From now on, we will call 'response factor' the reduced response factor defined as the real part of the transfer function Z :

$$\frac{N}{\alpha}=\Re(Z) \tag{21}$$

The response factor includes phase relations since it is positive when the vaporization rate and the chamber pressure are either above or below their mean values, and negative when the vaporization rate and the chamber pressure are on the opposite sides of their means [7]. Moreover, the phase difference ϕ between the vaporization rate and the chamber pressure, defined as $\phi=\arg(Z)$, is proved to remain insensitive to the chamber mean pressure magnitude [4]. Thus, the phase angle ϕ appears to be one of the key parameters for analysing the mass frequency response due to ambient pressure oscillations.

4 Results and discussion

In this section, all the calculations and curves are performed with the fuel thermodynamic coefficients $A=10$ and $B=100$. These parameter values correspond approximately to orders of magnitude of values encountered in the classical fuels [15]. The mass response factor of the mean droplet will be analysed relatively to the heat transfer coefficient h that controls the feeding regime, and to the process characteristic times as defined in subsection 2.2, and again to the influence of the value of the thermodynamic coefficient B. In each diagram on Figure 2, response factor curves are shown as function of the reduced frequency $u=3\omega\bar{\tau}_v$ for a set of values of the exchange ratio $\theta=9\bar{\tau}_v/\bar{\tau}_T$. For a given value of the heat transfer coefficient h, a quite large number of values of the exchange ratio θ are selected in order to illustrate a fairly wide range of curve profiles, among which the one corresponding to a certain critical value of θ to be later deduced in this analysis. The diagrams are ranged in five columns corresponding respectively to five different values of the heat transfer coefficient: $h=0;\ 0.1;\ 1;\ 10$ and $+\infty$. As already mentioned in the precedent section, the extreme values ($h=0$ and $h=+\infty$) are connected to the adiabatic and isothermal feeding regimes at the mean droplet centre and the related curves are here illustrated for comparison purposes with previous results obtained in [17]. Among the selected values ($h=0.1;\ 1;\ 10$), the value one is a particular value (see the discussion below) and can be roughly considered with the two other intermediate values as representative of the main types of curve profiles obtained for h varying from 0 to $+\infty$.

4.1 Effects of the heat transfer coefficient h

First, for $h=0$ (Figures 2(a1), 2(a2) and 2(a3)) and for $h\to+\infty$ (Figures 2(e1), 2(e2) and 2(e3)), the response factor curves seem respectively like those of the adiabatic and of the isothermal injection regimes discussed in [17].

In fact, these curves are identical since, for a given value of the exchange ratio θ, calculations show that

$$E(u,\theta,h) \to \frac{\bar{s}_0\bar{r}_S\theta\sin(\bar{s}_0\bar{r}_S)+2\theta\cos(\bar{s}_0\bar{r}_S)-3\cos(\bar{s}_0\bar{r}_S)-2\theta+3}{\theta(1-\cos(\bar{s}_0\bar{r}_S))} = E(u,\theta,0) \qquad (22)$$

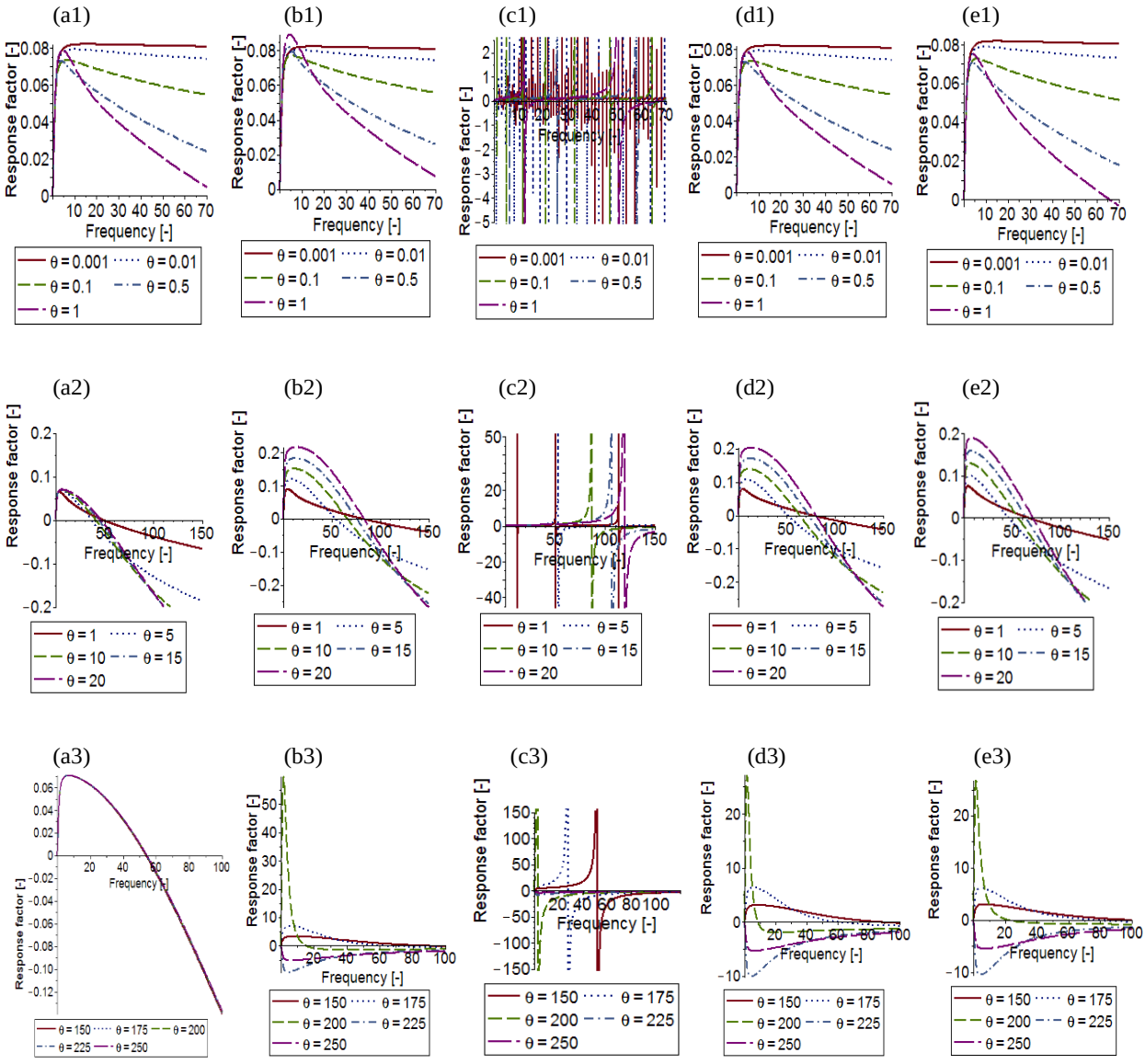

Figure 2. Effects of heat transfer coefficient h on the reduced response factor N/α of the mean spherical droplet with the fuel thermophysical properties $A=10$ and $B=100$. (a1), (a2) and (a3) for $h=0$ or adiabatic centre. (b1), (b2) and (b3) for $h=0.1$. (c1), (c2) and (c3) for $h=1$. (d1), (d2) and (d3) for $h=10$. (e1), (e2) and (e3) for $h=+\infty$ or isothermal centre.

when $h \to 0$, while

$$E(u,\theta,h) \to -\frac{1}{2}\frac{2\theta s_0\bar{r}_S\sin(s_0\bar{r}_S)+5\theta\cos(s_0\bar{r}_S)-3\cos(s_0\bar{r}_S)-5\theta+3}{\theta(1-\cos(s_0\bar{r}_S))} = E(u,\theta,+\infty) \qquad (23)$$

when $h \to +\infty$. The function $E(u,\theta,h)$ is defined in Equation (16) and mentioned in Equation (20). The above expressions of $E(u,\theta,0)$ and $E(u,\theta,+\infty)$ are exactly the same, compared with those obtained in [17] for the calculation of the complex transfer function Z in adiabatic and isothermal feeding regimes. Hence, all the results concerning the comparison of these two extreme cases of injection, as highlighted in this latter reference, are still valid for the present analysis.

Secondly, according to Figures 2(c1), 2(c2) and 2(c3), the response factor curves show intriguing fluctuations in their profiles when the value of the heat transfer coefficient h is fixed at one. In this case, if the value of the exchange ratio θ is chosen less than one, the oscillations become straight chaotic although they appear relatively reduced in amplitude contrary to those obtained when the exchange ratio θ is much greater than one. Indeed, keeping $h = 1$ and increasing the value of the exchange ratio θ beyond one until a certain threshold value to be later specified, a response factor line exhibits some hyperbolic pattern with high peaks value along the reduced frequency axis as in Figures 2(c2) and 2(c3).

Moreover, once the heat transfer coefficient slightly differs from one, the curves tend to show more lower fluctuations in their profiles even if h remains very close to one as for $h = 0.95$ or $h = 1.05$, and many other cases not illustrated with figures. In comparison, the unity value of a heat transfer coefficient may characterize radiation heat transfer processing from the flame to the chamber wall. According to [26] for example, the radiative power is highly nonlinear and varies at the first order as the fourth power of the local instantaneous temperature. It must be admitted that, even in fuel injection processes, this specific value of the liquid-liquid heat transfer coefficient ($h = 1$) can strongly influence the evaporating mass frequency response of spray droplets.

Thirdly, for a given value of the exchange ratio θ, almost identical curve profiles are obtained when the not null transfer coefficient h remains much less than one as for $0 < h \le 0.1$. Likewise, for $h \ge 10$, the response curve profiles seem unaffected by the variation of the transfer coefficient h at θ fixed. Indeed, Figures 2(d1), 2(d2) and 2(d3) for $h = 10$ show very similar profiles respectively with Figures 2(e1), 2(e2) and 2(e3) for $h = +\infty$. This behaviour can be explained by considering in the expression of the function $E(u,\theta,h)$ defined in Equation (16), the rate of variation of the term $\exp(\mathrm{i}\arctan h) = (\mathrm{i}h+1)/(h^2+1)^{1/2}$ or more precisely that of its inner function $\arctan(h)$. Since this rate of variation near $h = 0$ can be equated to one, the function $\arctan(h)$ tends rapidly enough to zero as h tends to zero. Consequently, the term $\exp(\mathrm{i}\arctan h)$ tends fast to one as h tends to zero. But, if the heat transfer coefficient h increases over one, the function $\arctan(h)$ tends asymptotically to the value $\pi/2$ which is yet approximately reached once the value of h is near 10. Then, the term $\exp(\mathrm{i}\arctan h)$ tends slowly to the imaginary number i. On one hand, the first limit leads to the expression of the function $E(u,\theta,0)$, giving in Equation (22) and corresponding to the transfer function Z for the adiabatic feeding regime. As this convergence is rapid, the curve profiles, although unaffected by the variation of h in the deleted neighbourhood of zero, seem noticeably different from those obtained for the adiabatic injection regime ($h = 0$). This is readily confirmed by comparison of Figures 2(a2) and 2(a3) with Figures 2(b2) and 2(b3), for respectively $h = 0$ and $h = 0.1$. On the other hand, the second limit leads to the expression of the function $E(u,\theta,+\infty)$ for the isothermal feeding regime (see Equation (23)). As the convergence is now asymptotic, the mass response factor curves for $h = 10$ seem very similar

to those obtained for the isothermal injection regime ($h=+\infty$). In brief, one may admit that, whenever the injection process is controlled by a positive heat transfer coefficient h, high and nonlinear instabilities may intervene in the vaporization frequency response of spray droplets. As a comparative example, the process of continuous supply of fuel to the chamber has been theoretically and experimentally identified as an important factor for producing or driving combustion instabilities [27, 28].

4.2 Effects of process characteristic times

The vaporization response of a LOX droplet to oscillatory ambient conditions has been computed over a wide range of frequencies and the results were applied to prototypical cases pertinent to liquid rocket combustion instabilities [6]. It has been shown that the peak frequency for the computed response factor is correlated to the droplet lifetime. Indeed, as already reported in [16, 17], the peak value of a response factor curve, whenever it exists, occurs at the same peak reduced frequency u_p about three. In mixed feeding regimes ($h>0$) as well as in both extreme cases of adiabatic and isothermal injection regimes, one has $u_p=3\omega\bar{\tau}_v\approx 3$ (see among others Figures 2(b1), 2(b2) for $h=0.1$ and 2(d1), 2(d2) for $h=10$). This relation implies $\bar{\tau}_v\approx 1/\omega$, meaning that the injected liquid residence time $\bar{\tau}_v$ is at the same order of magnitude as the oscillation period $1/\omega$. Now, the mean residence time $\bar{\tau}_v$ of a continuously fed droplet can be equated to the mean lifetime of free droplets in the spray. Therefore, whenever positive responses appear in the system, regardless of the value of the heat transfer coefficient $h\geq 0$, the vaporization rate can fully respond to the acoustic oscillations, only when the mean droplet lifetime equals the wave period of the ambient pressure oscillations.

It has also been anticipated that the well-known phase-lag model represents a key to a fundamental understanding of the evaporating mass frequency response to ambient pressure oscillations. Figure 3 shows phase angle $\phi=\arg(Z)$ curves as functions of the reduced frequency $u=3\omega\bar{\tau}_v$, for selected values of the exchange ratio $\theta=9\bar{\tau}_v/\bar{\tau}_T$. The curves are represented in a range of diagrams corresponding respectively to the same list of values of the heat transfer coefficient: $h=0;\ 0.1;\ 1;\ 10$ and $+\infty$ as retained for the illustration of response factor curves. For $h=0$ that is in the adiabatic feeding regime (see Figure 3(a)), phase angle curves collapse in a single line once $\theta\geq 1$, in accordance with the response factor curve profiles obtained in Figures 2(a1), 2(a2) and 2(a3). It is also remarkable that the cut-off frequency of this single curve is approximately equal to the peak frequency $u_p=3\omega\bar{\tau}_v\cong 3$ at which the vaporization rate oscillates in phase with the acoustic pressure ($\phi=0$). In the adiabatic regime, a typical phase-angle curve starts from $\pi/2$ at the frequency $u=0$ where the mass response is null, decreases rapidly to zero at the cut-off frequency u_p where the response is maximal, and then decreases asymptotically to a negative value about $-\pi/3$ expressing thus a progressive damp of instability in the system. Likewise, the phase-angle curves for $h=0.1$ and for $h=1$ as shown in Figures 3(b) and 3(c) are in agreement with the expectations. Phase-angle curve profiles obtained in Figure 3(d) for $h=10$ seem to be identical to those obtained in the isothermal feeding regime i.e. in Figure 3(e) corresponding to $h=+\infty$. As explained in the precedent subsection, this similitude is due to the asymptotical convergence of the function $\arctan(h)$ to the value $\pi/2$. On the other hand, an instantaneous change from the extreme value $-\pi$ to the other extreme value π is shown by these latter

phase-lag curves about the peak frequency u_p when the value of the exchange ratio θ approaches 200.

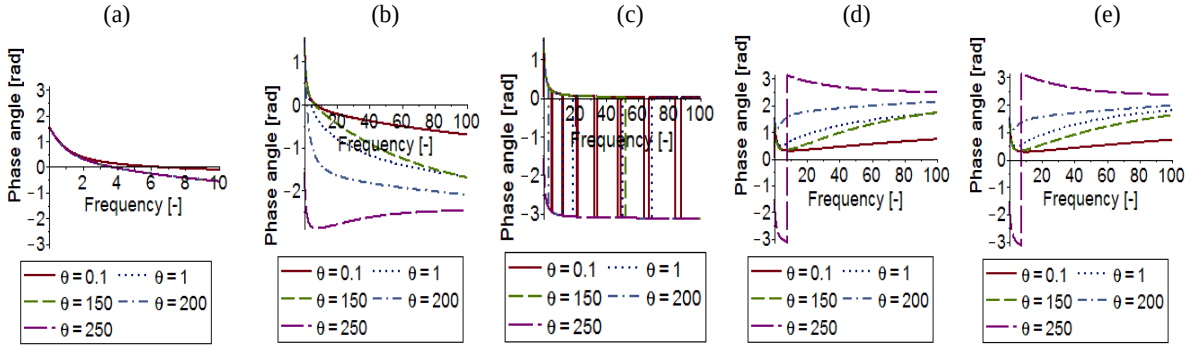

Figure 3. Influence of heat transfer coefficient h on phase lags of vaporization rate of the mean spherical droplet with the fuel thermophysical properties $A=10$ and $B=100$. (a) for $h=0$ or adiabatic centre. (b) for $h=0.1$. (c) for $h=1$. (d) for $h=10$. (e) for $h=+\infty$ or isothermal centre.

4.3 Influence of the value of the thermodynamic coefficient B

As they occur about a fixed value of the thermal exchange ratio ($\theta \approx 200$), the sharp changes noted in the response factor curve profiles are not related to some particular values of the heat transfer coefficient, but rather to a specific value of θ. As in [17], those rapid changes in curve profiles around the reduced frequency $u_p \approx 3$ can be proved as depending on a specific value of θ which is in connection with the value of the liquid fuel thermodynamic coefficient $B = 3\mu/\lambda$. In order to determine this threshold value θ_d of the thermal exchange ratio at which abrupt changes intervene in the curve profiles, the ratio $x = u/\theta = \omega\bar{\tau}_T/3$ may be particularly useful. Indeed, the thermal diffusion time $\bar{\tau}_T$ and the frequency of the oscillating wave ω do intervene in this ratio but not the residence time $\bar{\tau}_v$. This ratio can then be assumed negligible at the fixed peak frequency $u_p = 3\omega_p\bar{\tau}_{vp} \approx 3$, provided that the thermal transfer time by diffusion $\bar{\tau}_T$ is negligible compared either to the oscillation period $1/\omega_p$ or to the residence time $\bar{\tau}_{vp}$ as $1/\omega_p \approx \bar{\tau}_{vp}$ at u_p. Therefore, whenever $h>0$, the second-order truncated expansion of the transfer function $Z(u,\theta,h)$ in the neighbourhood of $x=0$, while assuming u closer to u_p, leads to the expression:

$$Z(u,\theta,h) \approx \frac{iu\left(A+\frac{\theta}{2}-\frac{3}{2}\right)}{(1+iu)\left(B-\frac{\theta}{2}+\frac{3}{2}\right)} \qquad (24)$$

This no more depends on the heat transfer coefficient h. But, when $h=0$ i.e. in the adiabatic regime, the computation leads to the following approximation: $Z(u,\theta,0) \approx iu(A-3)/[(1+iu)(B+3)]$. In consequence, once the feeding process is controlled by a positive heat transfer coefficient, the value of θ around which mass response factor curves exhibit the sharp peak at the frequency u_p, can be deduced from the estimation (24) by equating the denominator of the right-hand side term to zero. Thus, $\theta_d = 2B+3 = 203$ for

$B = 100$. Moreover, once the value of θ exceeds θ_d, one has $\Re(Z) \leq 0$ whenever $h > 0$, as it can be equally deduced from the right-hand side term of the same estimation (24). Therefore, the corresponding response factor curves only show negative response for all frequencies as shown in Figures 2(b3), 2(c3) and 2(d3) for h = 0.1; 1 and 10 respectively. As in [4, 29], many publications have highlighted that the rapid variations of fluid thermophysical properties near critical and supercritical vaporization processes are the major factor contributing to abrupt changes in droplets frequency response. However, as shown by the present study, an abrupt or a completely damped vaporization frequency response may occur during subcritical combustion processes, provided that certain specific boundary conditions are imposed.

5 Conclusions

By introducing a heat transfer coefficient in the liquid fuel injection process, this study has extended to a more generalized feeding regime the results of the pressure-coupled vaporization frequency response of spray droplets. An idealized configuration of the mean droplet has permitted to analyse the evaporating mass frequency response of the spray of repetitively injected droplets in the combustion chamber. The effects of the liquid heat transfer coefficient and of the process characteristic times, as well as those of the thermal exchange ratio are found effective for driven or dampen instabilities. It was shown that, whenever positive responses appear in the system, the peak value is reached at a particular frequency, where the residence time of the mean droplet matches the period of the ambient pressure oscillations. Except for the case where the heat transfer coefficient is equal to one, response factor curves exhibit a single abrupt peak response at the involved particular frequency. Moreover, the single abrupt peak response grows exponentially at the particular frequency if the thermal exchange ratio approaches a certain threshold value. The latter is shown equal to a simple affine function of a thermodynamic coefficient related to fuel physical properties. Once this threshold value of the thermal exchange ratio is passed over, a factor curve shows only negative response for all frequencies even if the heat transfer coefficient value equals one. The results are also found similar to those previously obtained in the adiabatic and isothermal feeding regimes. Mass response factors in such extreme cases of fuel injection are recovered as simple limit points. The above-mentioned results may be beneficial for instability control in combustion processes and also for liquid fuel propulsion systems.

References

[1] V. Nair and R. I. Sujith, *Multifractality in combustion noise: Predicting an impending instability*, J. Fluid Mech. 747 (2014), pp. 635–655.

[2] T. Pant, C. Han, and H. Wang, *Computational investigations of the coupling between transient flame dynamics and thermo-acoustic instability in a self-excited resonance combustor*, Combust. Theory Model. (23)5 (2019), pp. 1-31.

[3] S. Candel, D. Durox, T. Schuller, N. Darabiha, L. Hakim, and T. Schmitt, *Advances in combustion and propulsion applications*, Eur. J. Mech. B Fluids 40 (2013), pp. 87-106.

[4] G.C. Hsiao, H. Meng, and V. Yang, *Pressure-coupled vaporization response of n-pentane fuel droplet at subcritical and supercritical conditions*, Proc. Combust. Inst. 33(2) (2011), pp. 1997–2003.

[5] S. Lei and A. Turan, *Chaotic modeling and control of combustion instability due to vaporization*, Int. J. Heat Mass Transf. 53(21-22) (2010), pp. 4482–4494.

[6] W. A. Sirignano, J.-P. Delplanque, C.H. Chiang, and R. Bhatia, *Liquid-propellant droplet vaporization: A rate controlling process for combustion instability*, in, *Liquid Rocket Engine Combustion Instability*, V. Yang and W. E. Anderson, eds., AIAA Publishers, Reston, 1994, pp. 307-343.

[7] L. Rayleigh, *Theory of Sound* (two volumes), Dover Publications, New York, 1877, Re-issued 1945.

[8] A. Duvvur, C.H. Chiang, and W.A. Sirignano, *Oscillatory fuel droplet vaporization: Driving mechanism for combustion instability*, J. Propul. Power 12(2) (1996), pp. 358-365.

[9] L. Yuan, C. Shen, and Z. Xinqiao, *Dynamic response of vaporizing droplet to pressure oscillation*, Heat Mass Transf. 52(2) (2017), pp. 711-723.

[10] A. Y. Tong and W.A. Sirignano, *Oscillatory vaporization of fuel droplets in an unstable combustor*, J. Propul. Power 5(3) (1989), pp. 257-261.

[11] M. de la Cruz Garc´ıa, E. Mastorakos, and A.P. Dowling, *Investigations on the self-excited oscillations in a kerosene spray flame*, Combust. Flame 156 (2009), pp. 175-186.

[12] C.T. Haddad and J. Majdalani, *Transverse waves in simulated liquid rocket engines*, AIAA J. 51(3) (2012), pp. 591-605.

[13] J. B. Greenberg and D. Katoshevski, *Polydisperse spray diffusion flames in oscillating flow*, Combust. Theory Model. 20(2) (2016), pp. 349-372.

[14] M.F. Heidmann and P.R. Wieber, *Analysis of frequency response characteristics of propellant vaporization*, Tech. Rep. TN D-3749, NASA, Washington D.C., USA, 1966.

[15] R. Prud'homme, M. Habiballah, L. Matuszewski, Y. Mauriot, and A. Nicole, *Theoretical analysis of dynamic response of a vaporizing droplet to a acoustic oscillation*, J. Propul. Power 26(1) (2010), pp. 74-83.

[16] K. Anani and R. Prud'homme, *Theoretical analysis of thermal conduction effect on frequency response of a perturbed vaporizing spherical droplet*, Flow Turbul. Combust. 98(2) (2017), pp. 503–522.

[17] K. Anani, R. Prud'homme, and M. N. Hounkonnou, *Dynamic response of a vaporizing spray to pressure oscillations: Approximate analytical solutions*, Combust. Flame 193 (2018), pp. 295-305.

[18] S.Y. Slavyanov and W. Lay, *The Heun class of equations*, in, *Special Functions: A Unified Theory Based on Singularities*, Oxford Math. Monogr., Oxford University Press Publishers, New York, 2000, pp. 97-162.

[19] J. G. Lee and D. A. Santavicca, *Experimental diagnostics of combustion instabilities*, in, *Combustion instabilities in gas turbine engines: Operational Experience, Fundamental Mechanisms, and Modelling*, T. C. Lieuwen and V. Yang, eds., AIAA Publishers, 2005, pp. 481-530.

[20] C. I. Sevilla-Esparza, J. L. Wegener, S. Teshome, J. I. Rodriguez, O. I. Smith, and A. R. Karagozian, *Droplet combustion in the presence of acoustic excitation*, Combust. Flame 161(6) (2014), pp. 1604-1619.

[21] F. Laurén and J. Nordström, *Practical inlet boundary conditions for internal flow calculations*. Comput. & Fluids 175 (2018), pp. 159-166.

[22] S. Bari, T.H. Lim, and C.W. Yu, *Effects of preheating of crude palm oil (CPO) on injection system, performance and emission of a diesel engine*, Renewable Energy 27(3) (2002), pp 339–351.

[23] S. Mondal, A. Mukhopadhyay, and S. Sen, *Effects of inlet conditions on dynamics of a thermal pulse combustor*, Combust. Theory Model. 16(1) (2012), pp. 59-74.

[24] R.S. Miller, K. Harstad, and J. Bellan, *Evaluation of equilibrium and non-equilibrium evaporation models for many droplet gas-liquid flow simulations*, Int. J. Multiph. Flow 24(6) (1998), pp. 1025-1055.

[25] B. Abramzon and W. A. Sirignano, *Droplet vaporization model for spray combustion calculations*, Int. J. Heat Mass Transf. 32(9) (1989), pp. 1605-1618.

[26] R. G. D. Santos, M. Lecanu, S. Ducruix, O. Gicquel, E. Iacona, and D. Veynante, *Coupled large eddy simulations of turbulent combustion and radiative heat transfer*, Combust. Flame 152(3) (2008), pp. 387–400.

[27] Y. Xu, M. Zhai, P. Dong, F. Wang, and Q. Zhu, *Modeling of a self-excited pulse combustor and stability analysis*, Combust. Theory Model. 15(5) (2011), pp. 623-643.

[28] A. Kannan, B. Chellappan, and S. Chakravarthy, *Flame-acoustic coupling of combustion instability in a non-premixed backward-facing step combustor: The role of acoustic-Reynolds stress*, Combust. Theory Model. 20(4) (2016), pp. 658-682.

[29] J. Ren, O. Marxen, and R. Pecnik, *Boundary-layer stability of supercritical fluids in the vicinity of the Widom line*, J. Fluid Mech. 871 (2019), pp. 831–864.